CLIMATOLOGY

Abrupt shift to hotter and drier climate over inner East Asia beyond the tipping point

Peng Zhang[1,2], Jee-Hoon Jeong[1]*, Jin-Ho Yoon[3], Hyungjun Kim[4], S.-Y. Simon Wang[5], Hans W. Linderholm[2], Keyan Fang[6,2], Xiuchen Wu[7,8], Deliang Chen[2]

Unprecedented heatwave-drought concurrences in the past two decades have been reported over inner East Asia. Tree-ring–based reconstructions of heatwaves and soil moisture for the past 260 years reveal an abrupt shift to hotter and drier climate over this region. Enhanced land-atmosphere coupling, associated with persistent soil moisture deficit, appears to intensify surface warming and anticyclonic circulation anomalies, fueling heatwaves that exacerbate soil drying. Our analysis demonstrates that the magnitude of the warm and dry anomalies compounding in the recent two decades is unprecedented over the quarter of a millennium, and this trend clearly exceeds the natural variability range. The "hockey stick"–like change warns that the warming and drying concurrence is potentially irreversible beyond a tipping point in the East Asian climate system.

Global warming has led to a shift in the probability distribution of summer temperatures (*1*), causing more frequent summer heatwaves in the Northern Hemisphere midlatitudes (*2*, *3*). Diverse and complex regional or global feedback mechanisms determine the magnitude of changes in heatwave frequency and regionality (*4*–*9*). In addition to the emergence of heatwave-prone atmospheric stagnation, soil moisture deficit before or during droughts has been identified as a key factor exacerbating heatwaves through the land-atmosphere coupling (*10*–*14*). This drought-heatwave interaction is particularly pronounced in semiarid regions such as southern Europe, western North America, and inner East Asia (Mongolia and northern China), where the land-atmosphere coupling is strong (*15*–*20*).

Although increasing concentration of greenhouse gases may enhance soil moisture deficits and heatwave occurrences in a warmer climate (*21*–*23*), the extent to which summer heatwaves are affected by the global warming–induced soil moisture reduction in a long-term context remains unclear. In this study, we used tree-ring data to reconstruct both heatwave frequency and soil moisture variability in inner East Asia, centered over Mongolia, for the past 260 years. We found a robust tendency toward a hotter and drier climate, with a stronger coupling of heatwave and drought in recent decades that was not observed before the 1990s. This trend, which was found in both observations and reconstructions, is likely associated with an enhanced land-atmosphere coupling associated with persistent soil moisture deficit.

Inner East Asia, including Mongolia and its surroundings (Fig. 1), features arid and semiarid climates where annual precipitation is <300 mm. It is one of the hotspots showing the strongest warming in the latter part of the 20th century (*24*). The frequency of summer heatwaves in this region has increased significantly during the past two decades (Fig. 1A). Concurrently, soil moisture content has shown a significant drying trend (Fig. 1B), which is consistent with previous studies based on observation and land surface modeling (*25*–*27*) (also see fig. S1).

To determine whether this modern-era drying falls within or outside the range of long-term natural variability, we reconstructed summer heatwave and soil moisture variations based on independent tree-ring chronologies sampled in inner East Asia (see the supplementary materials).

[1]Faculty of Earth and Environmental Sciences, Chonnam National University, Gwangju, Korea. [2]Regional Climate Group, Department of Earth Sciences, University of Gothenburg, Gothenburg, Sweden. [3]School of Earth Sciences and Environmental Engineering, Gwangju Institute of Science and Technology, Gwangju, Korea. [4]Institute of Industrial Science, The University of Tokyo, Tokyo, Japan. [5]Department of Plants, Soils and Climate/Utah Climate Center, Utah State University, Logan, UT, USA. [6]Key Laboratory of Humid Subtropical Eco-Geographical Process (Ministry of Education), College of Geographical Sciences, Fujian Normal University, Fuzhou, China. [7]State Key Laboratory of Earth Surface Processes and Resource Ecology, Beijing Normal University, Beijing, China. [8]Faculty of Geographical Science, Beijing Normal University, Beijing, China.
*Corresponding author. Email: jjeehoon@jnu.ac.kr

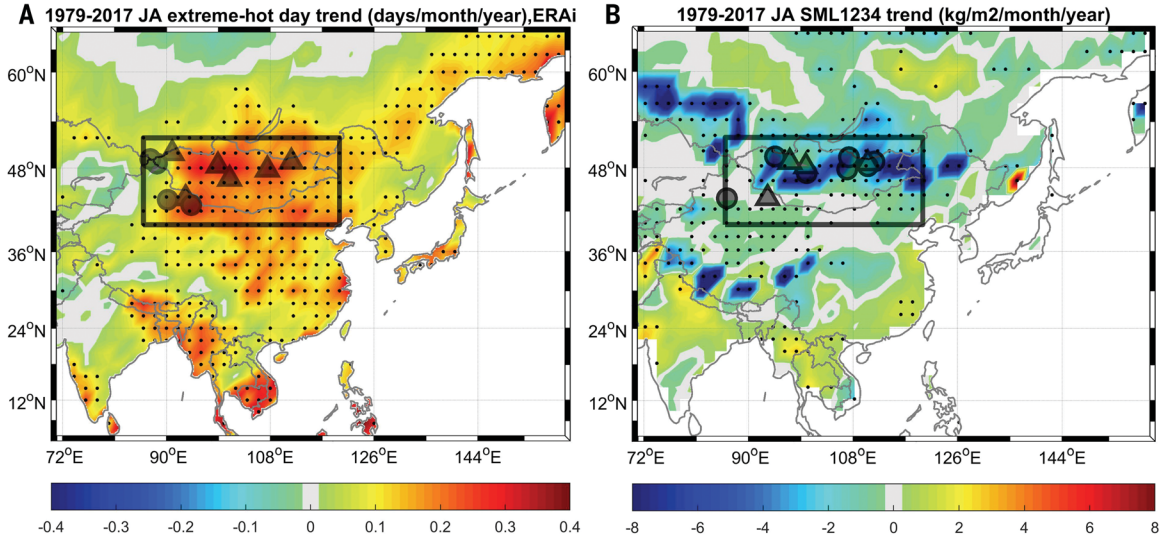

Fig. 1. Trends of hot day frequency and soil moisture content. (**A** and **B**) Trends of July-August mean extremely hot day frequency (A) and soil moisture content (B) in 1979–2017. Black frame marks the defined domain of inner East Asia. Black dots mark the grids where the trends are significant at the $P < 0.05$ level. Triangles and circles mark the locations where the tree-ring data were used to reconstruct the extremely hot day frequency and soil moisture variability on interannual and above-interannual time scale, respectively.

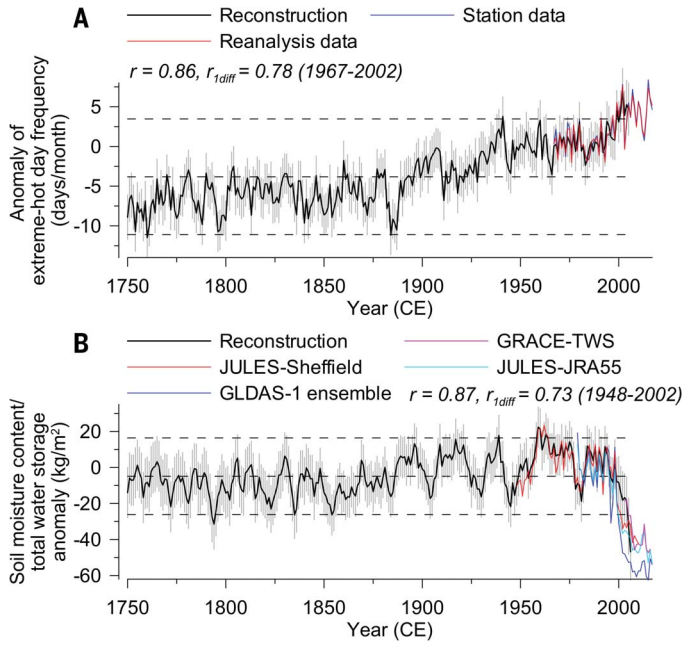

Fig. 2. Tree-ring width–based reconstructions. (**A** and **B**) Tree-ring width–based reconstructions of July-August mean extremely hot day frequency (A) and soil moisture anomaly (B) in 1750–2002 in inner East Asia (solid black curves) and their uncertainty (gray bars, defined as 2σ of reconstruction ensembles). The red and blue curves in (A) are the extremely hot day frequency variability derived from ERA interim and station datasets. The red, cyan, blue, and pink curves in (B) are the soil moisture anomaly derived from the JULES-Sheffield (1948–2010), JULES-JRA55 (1979–2017), and GLDAS-1 (ensemble mean, 1979–2017), and total water storage anomaly (relative to a value of −35kg/m^2) derived from the Gravity Recovery and Climate Experiment (GRACE) mission over 2002–2016 (for details, see the supplementary materials; note that there are data missing in August of 2013 and July of 2014), respectively. Dashed horizontal lines represent the long-term mean and ±2σ over the period 1750–2002. The correlation coefficients (*r*) are calculated between the reconstruction and the reanalysis data in (A) and between the reconstruction and JULES-Sheffield soil moisture in (B). r_{1diff} is the correlation coefficient of the first difference of time series.

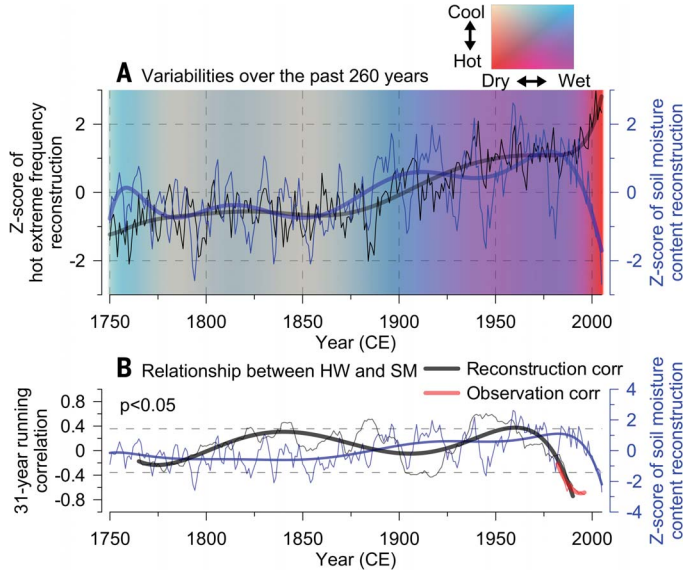

Fig. 3. Comparison of data over the past 260 years. Shown is a comparison between the July-August mean extremely hot day frequency variability and soil moisture variability in inner East Asia over the past 260 years. (**A**) Variability of the reconstructed extremely hot day frequency (black) and soil moisture content (blue) and their low-frequency variations over the past 260 years. (**B**) Thirty-one-year running correlation between hot extreme frequency and soil moisture over 1750–2005 based on the reconstructions (black curves) and over 1967–2011 based on reanalysis and JULES-Sheffield data (red curve), where the light dashed lines indicate the $P < 0.05$ significance level. The blue curves are the soil moisture reconstruction; bold curves are their low-frequency variations.

The heatwave reconstruction in Fig. 2A, explaining 74% of the variance in the instrumental heatwave record for the period 1967–2002, shows a weak long-term change before the 20th century. Subsequently, it displays a gradual increase until the 1950s, followed by a phase of pronounced increase since the 1970s. The elevated heatwave frequency in recent decades appears to exceed that of natural variability in the context of the past 260 years. This result echoes previous summer temperature reconstructions in the same region (*28*).

The soil moisture reconstruction in Fig. 2B, which explains 76% of the variance in observed soil moisture over the period 1948–2002, shows a negligible trend until the end of the 20th century, after which its accelerated decline becomes evident. It should be noted that the reconstructed and simulated soil moisture records reveal periods of reductions in the 1900s, 1920s, 1940s, and 1970s that are in good agreement with documented megadrought events in Mongolia (*29*–*31*) (also see fig. S2). However, the post–20th-century reduction of soil moisture reached a record low, plummeting below the −2 SD level. This is consistent with other soil moisture datasets and a satellite-based total water storage observation (Fig. 2B; also see the supplementary materials), suggesting an abrupt and unprecedented drying trend.

When the reconstructions of heatwave frequency and soil moisture are compared (Fig. 3A), a substantial shift toward a "drier-hotter" regime from the late 20th century onward is apparent. This latter regime is unusual because before the 1950s, the two variables shared a more or less coherent long-term change in which both were increasing. In summer, a dry soil condition can exert heat into the lower atmosphere through sensible heat flux while suppressing evaporative cooling, so positive feedback between droughts and near-surface warming can be triggered by the soil moisture deficit reaching certain thresholds. Over multidecadal time scales, heatwave frequency and soil moisture exhibit a weak anticorrelation ($r = -0.05$, $P > 0.1$) until the mid-20th century (thick lines in Fig. 3A). In the past 260 years, only the recent decades show a significant anticorrelation between heatwave frequency and soil moisture, alongside a radical decline in soil moisture (Fig. 3B). The observation of the compound warming and drying is unprecedented in inner East Asia, implying a regime change in the regional land-atmosphere coupling. The upshot of this result is that the regional near-surface air may have increased its sensitivity to soil moisture fluctuation. A series of recent heatwave events in Europe (*32*) and North America (*18*) have revealed this phenomenon, suggesting that the semiarid climate of this region has

entered a new regime in which soil moisture no longer mitigates anomalously high air temperature.

To attribute the apparent increase in the heatwave-drought concurrence to regional climate variability, we investigated the changes in the large-scale atmospheric circulation and the impact of the land feedback. Figure 4, A and B, show composite maps of geopotential height (GPH) and wind anomalies at 500 hPa for the years of unusually high heatwave frequency for two periods, 1979–1998 and 1999–2017. In both periods, a large-scale wave train spanning northern Eurasian continent is revealed, with prominent high-pressure anomalies over the study area, which has been noted previously (*33*). In the latter period, the pattern of amplified high-pressure anomalies is consistent with the observed trends in the summer upper-air circulations (*34*).

Figure 4, C and D, show the vertical sections of the high-pressure ridge across inner East Asia in terms of GPH and air temperature, depicting the warm-core feature of the drought-heatwave accompanying the high-pressure anomaly that has intensified in the latter period. Even though that amplified upper-tropospheric wave train (*34*) has contributed to this feature, the fact that increased land surface warming also extends upward into the middle troposphere in Fig. 4D suggests an intensified land-atmosphere coupling. This claim is linked to the aforementioned soil moisture deficit trend causing the drier land surface to produce stronger sensible heat flux into the lower atmosphere, which thickens the planetary boundary layer and therefore amplifies the upper-air high pressure (*35*). As part of the positive feedback, the strengthened anticyclone aloft further increases surface warming through enhanced downward shortwave radiation. Recent megaheatwaves in Europe (e.g., those in 2003 and 2010) have been attributed to similar land-atmospheric couplings and atmospheric feedbacks that exacerbate the heatwaves (*11–13*, *36–39*).

The recent change in land-atmosphere coupling can be quantified using the π diagnostic of soil moisture–temperature coupling (*13*) (see the supplementary materials). This metric quantifies the relation between near–surface temperature anomalies and soil moisture deficits in the land surface energy balance. During the past two decades, the strength of the land-atmosphere coupling has been profoundly enhanced over a large part of Asia, including southeastern Asia, China, and Mongolia (Fig. 5, A and B). The most extensive change occurred over Mongolia and northern China (Fig. 5C),

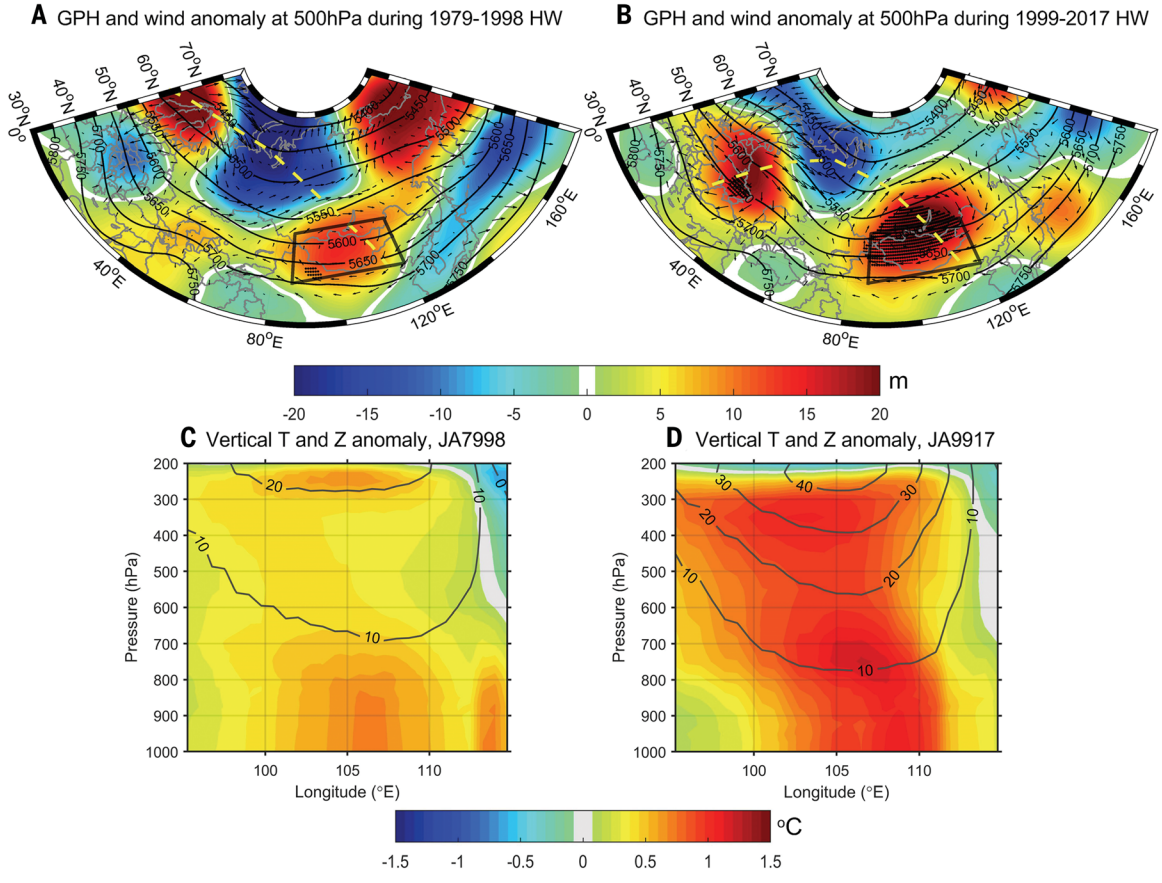

Fig. 4. Composite map. (**A** and **B**) Composite map of July-August mean geopotential height and wind anomalies at 500 hPa for the years when extremely hot day frequency was anomalously high (>0.4σ; the results are not sensitive to the threshold) over the period 1979–1998 [the selected years are 1980, 1987, 1989, 1991, 1996, and 1997 (A)] and 1999–2017 [the selected years are 1999, 2001, 2002, 2007, 2010, 2015, and 2016 (B)] and their corresponding vertical structures of temperature and geopotential height. Contour lines show climatology of the geopotential height, and black stripes mark the areas where pressure change is significant at the $P < 0.05$ level calculated based on the Monte Carlo method with 1000 iterations. Yellow dashed line denotes the track of the wave train pattern. Black frame marks the defined domain of inner East Asia. (**C** and **D**) Lower panels show corresponding vertical structures of temperature (shading) and geopotential height anomalies (contour lines in meters) along the wave train tracks in inner East Asia over the period of 1979–1998 (C) and 1999–2017 (D). The geopotential height, wind, and temperature data are derived from ERA interim monthly dataset with 0.75° latitude × 0.75° longitude resolution and 23 pressure levels from 200 up to 1000 hPa.

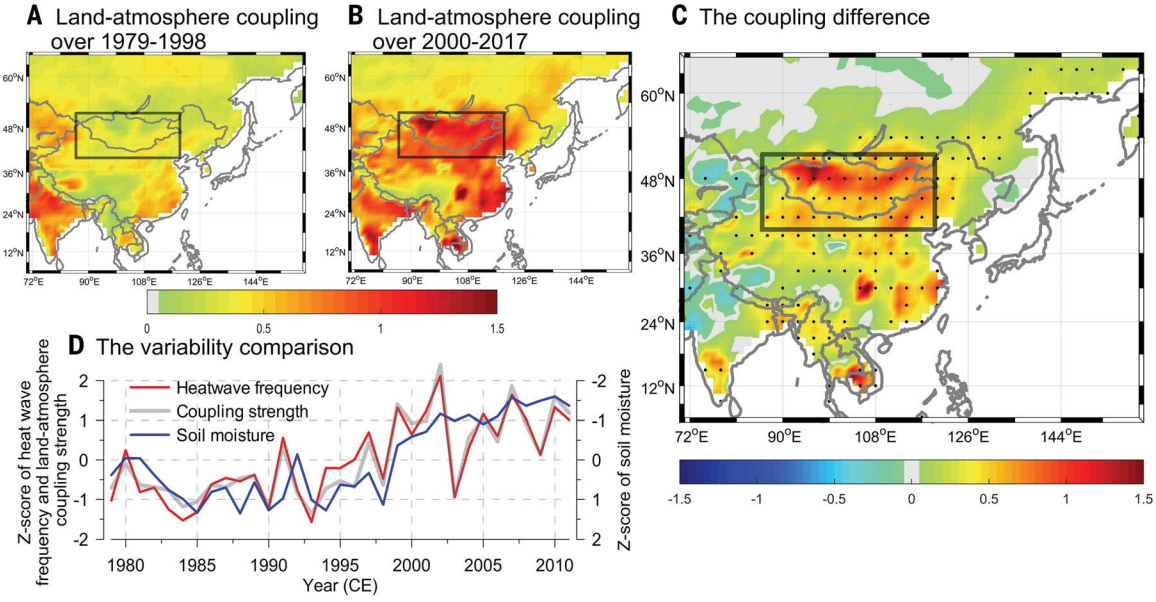

Fig. 5. Land-atmosphere coupling strength. (**A** to **C**) July-August land-atmosphere coupling strength over the period 1979–1998 (A) and 2000–2017 (B) and their differences [(B) minus (A)] (C) and comparison with soil moisture and heatwave frequency variabilities. Black dots mark the grids where differences are significant at the $P < 0.05$ level. The coupling strength is calculated based on the ERA interim daily dataset with 1.5° latitude × 1.5° longitude spatial resolution. (**D**) Interannual variability of the coupling strength (gray), hot extreme frequency (red), and soil moisture (blue, reversed value in *y*-axis) over the domain.

where a robust trend of drier-hotter air under the strengthened anticyclone was observed. The temporal variation of the coupling strength is almost identical to the heatwave frequency and also matches the continuous drying trend of soil moisture (Fig. 5D). The uptrend of the association between heatwave frequency and land-atmosphere coupling follows the persistent change in soil moisture deficit. This feature is not as robust over southern and coastal East Asia, where the local climate is largely influenced by the East Asia summer monsoon (*40*).

Tree-ring and observational evidence show that the increased frequency of summer heatwaves and the concurrent increase in severe droughts over inner East Asia in recent decades are unique in a 260-year context. Given the enhanced land-atmosphere interaction associated with the continuously drying soil, the land-atmosphere coupling over inner East Asia might have entered a different regime in which the soil moisture variability has become too small and the sensitivity of evaporation to more dryness has weakened (fig. S3). Such a regime shift would explain why heatwaves and droughts have become tightly coupled and can quickly enhance each other, leading to an increase in concurrent events of heatwave and drought. Although our analysis does not include a future projection, it can be expected that the "regime shift," which is supported by multiple lines of evidence, gives way to a new state in which there are stronger negative associations between heatwaves and soil moisture that are expected to persist under a warmer climate. The implication of these findings is that compound extremes of summer heatwaves and heatwave-droughts may occur more frequently and potentially become more severe in inner East Asia, and that corresponding mitigation efforts should be undertaken to cope with the associated increase in the risk of livestock and rangeland crisis in Mongolia.

REFERENCES AND NOTES

1. K. A. McKinnon, A. Rhines, M. P. Tingley, P. Huybers, *J. Geophys. Res. Atmos.* **121**, 8849–8868 (2016).
2. N. Christidis, G. S. Jones, P. A. Stott, *Nat. Clim. Chang.* **5**, 46–50 (2015).
3. D. Coumou, S. Rahmstorf, *Nat. Clim. Chang.* **2**, 491–496 (2012).
4. R. García-Herrera, J. Díaz, R. M. Trigo, J. Luterbacher, E. M. Fischer, *Crit. Rev. Environ. Sci. Technol.* **40**, 267–306 (2010).
5. J. Cohen *et al.*, *Nat. Geosci.* **7**, 627–637 (2014).
6. Q. Tang, X. Zhang, J. A. Francis, *Nat. Clim. Chang.* **4**, 45–50 (2014).
7. N. Pepin *et al.*, *Nat. Clim. Chang.* **5**, 424–430 (2015).
8. D. Coumou, J. Lehmann, J. Beckmann, *Science* **348**, 324–327 (2015).
9. Z. Wu, P. Zhang, H. Chen, Y. Li, *Clim. Dyn.* **46**, 3405–3417 (2016).
10. R. Vautard *et al.*, *Geophys. Res. Lett.* **34**, L07711 (2007).
11. E. M. Fischer, S. I. Seneviratne, P. L. Vidale, D. Lüthi, C. Schär, *J. Clim.* **20**, 5081–5099 (2007).
12. E. M. Fischer, S. I. Seneviratne, D. Lüthi, C. Schär, *Geophys. Res. Lett.* **34**, L06707 (2007).
13. D. G. Miralles, A. J. Teuling, C. C. Van Heerwaarden, J. Vilà-Guerau de Arellano, *Nat. Geosci.* **7**, 345–349 (2014).
14. J. Zscheischler, S. I. Seneviratne, *Sci. Adv.* **3**, e1700263 (2017).
15. R. D. Koster *et al.*, *Science* **305**, 1138–1140 (2004).
16. M. Hirschi *et al.*, *Nat. Geosci.* **4**, 17–21 (2011).
17. S. D. Schubert, H. Wang, R. D. Koster, M. J. Suarez, P. Y. Groisman, *J. Clim.* **27**, 3169–3207 (2014).
18. R. Saini, G. Wang, J. S. Pal, *J. Hydrometeorol.* **17**, 2191–2207 (2016).
19. T. Cowan *et al.*, *J. Clim.* **30**, 2437–2461 (2017).
20. E. Erdenebat, T. Sato, *Atmos. Sci. Lett.* **17**, 135–140 (2016).
21. G. Zittis, P. Hadjinicolaou, M. Fnais, J. Lelieveld, *Reg. Environ. Change* **16**, 1863–1876 (2016).
22. J. Lelieveld *et al.*, *Clim. Change* **137**, 245–260 (2016).
23. V. Humphrey *et al.*, *Nature* **560**, 628–631 (2018).
24. D. L. Hartmann, A. Klein Tank, M. Rusticucci, L. Alexander, S. Broennimann, Y. A.-R. Charabi, F. Dentener, E. Dlugokencky, D. Easterling, A. Kaplan, B. Soden, P. Thorne, M. Wild, P. Zhai, J. Hurrell, J. A. Marengo Orseni, F. Tangang, P. Viterbo, "Observations: atmosphere and surface" in *Climate Change 2013 – The Physical Science Basis: Contributions of Working Group I Contribution to the Fifth Assessment Report of the Intergovernmental Panel on Climate Change*, T. F. Stocker, D. Qin, G.-K. Plattner, M. M. B. Tignor, S. K. Allen, J. Boschung, A. Nauels, Y. Xia, V. Bex, P. M. Midgley, Eds. (Cambridge Univ. Press, 2013), pp. 187–201.
25. M. Rodell *et al.*, *Bull. Am. Meteorol. Soc.* **85**, 381–394 (2004).
26. M. Rodell *et al.*, *Nature* **557**, 651–659 (2018).
27. B. R. Scanlon *et al.*, *Proc. Natl. Acad. Sci. U.S.A.* **115**, E1080–E1089 (2018).
28. E. R. Cook *et al.*, *Clim. Dyn.* **41**, 2957–2972 (2013).
29. E. R. Cook *et al.*, *Science* **328**, 486–489 (2010).
30. N. Pederson, A. E. Hessl, N. Baatarbileg, K. J. Anchukaitis, N. Di Cosmo, *Proc. Natl. Acad. Sci. U.S.A.* **111**, 4375–4379 (2014).
31. A. E. Hessl *et al.*, *Sci. Adv.* **4**, e1701832 (2018).
32. S. I. Seneviratne, D. Lüthi, M. Litschi, C. Schär, *Nature* **443**, 205–209 (2006).
33. M. P. Rao *et al.*, *Environ. Res. Lett.* **10**, 074012 (2015).
34. S. Y. Wang, R. E. Davies, R. R. Gillies, *J. Geophys. Res. Atmos.* **118**, 11059–11074 (2013).
35. S. Y. S. Wang *et al.*, *J. Geophys. Res. Atmos.* **120**, 8804–8816 (2015).
36. R. Lorenz, E. B. Jaeger, S. I. Seneviratne, *Geophys. Res. Lett.* **37**, L09703 (2010).
37. M. Stéfanon, P. Drobinski, F. D'Andrea, C. Lebeaupin-Brossier, S. Bastin, *Clim. Dyn.* **42**, 1309–1324 (2014).
38. M. Hauser, R. Orth, S. I. Seneviratne, *Geophys. Res. Lett.* **43**, 2819–2826 (2016).
39. E. Seo *et al.*, *Clim. Dyn.* **52**, 1695–1709 (2019).
40. D. Yihui, J. C. L. Chan, *Meteorol. Atmos. Phys.* **89**, 117–142 (2005).

41. P. Zhang, JULES-Sheffield soil moisture 1948-2010, figshare (2020); https://figshare.com/articles/dataset/JULES-Sheffield_soil_moisture_1948-2010/13040534.
42. P. Zhang, JULES-JRA55 soil moisture 1979-2017, figshare (2020); https://figshare.com/articles/dataset/JULES-JRA55_soil_moisture_1979-2017/13040540.

ACKNOWLEDGMENTS

We thank M.-S. Kim for collection and preprocessing of tree ring data; K.-M. Kim for providing JULES-Sheffield and JULES-JRA55 soil moisture data; colleagues and friends for valuable discussions on the results of this study; and the scientists who shared their valuable tree ring width data from ITRDB used in this study. **Funding:** This work was supported by the Korea Meteorological Administration Research and Development Program under grant no. KMI2018-07010; the Strategic Priority Research Program of the Chinese Academy of Sciences under grant no. XDA20060400; and by the Swedish Research Council for Sustainable Development (FORMAS) under grant no. 2018-02858. H.W.L. was supported by the Swedish Research Council (VR; grant nos. 2012-05246 and 2015-04031). This is a contribution to the Swedish BECC and MERGE. H.K. acknowledges Grant-in-Aid for Specially Promoted Research 16H06291 and 18KK0117 from the Japan Society for the Promotion of Science. S.-Y.S.W. is supported by NSF p2c2 award no. 1903721. **Author contributions:** P.Z. and J.-H.J. designed the research, conducted analyses, and wrote most of the manuscript content. S.-Y.S.W., J.-H.Y., and H.K contributed to analysis and did most of the report writing. H.W.L, K.F., X.W., and D.C. contributed to analysis and report writing. All authors discussed the study results and reviewed the manuscript. **Competing interests:** The authors declare no competing interests. **Data and materials availability:** All data used in this study are freely accessible. Tree-ring data can be downloaded from International Tree-Ring Data Bank at https://www.ncdc.noaa.gov/data-access/paleoclimatology-data/datasets/tree-ring (see the materials and methods for details about the tree-ring data used in this study). GLDAS soil moisture data are freely available online at https://ldas.gsfc.nasa.gov/gldas or through an interactive online application Giovanni (https://giovanni.gsfc.nasa.gov/giovanni/#). JULES-Sheffield (*41*) and JULES-JRA55 (*42*) soil moisture data can be found at figshare. ERA-interim and ERA-40 daily reanalysis datasets are available at https://www.ecmwf.int/en/forecasts/datasets/browse-reanalysis-datasets. GRACE-TWS data are available at https://grace.jpl.nasa.gov/data/get-data/jpl_global_mascons/. The Global Historical Climate Network Daily (GHCN-D) dataset can be downloaded from https://www.ncdc.noaa.gov/ghcn-daily-description.

SUPPLEMENTARY MATERIALS

science.sciencemag.org/content/370/6520/1095/suppl/DC1
Materials and Methods
Figs. S1 to S6
Table S1
References (*43*–*73*)

17 February 2020; accepted 12 October 2020
10.1126/science.abb3368

Science

Abrupt shift to hotter and drier climate over inner East Asia beyond the tipping point

Peng Zhang, Jee-Hoon Jeong, Jin-Ho Yoon, Hyungjun Kim, S.-Y. Simon Wang, Hans W. Linderholm, Keyan Fang, Xiuchen Wu and Deliang Chen

Science **370** (6520), 1095-1099.
DOI: 10.1126/science.abb3368

A dangerous trend

How anthropogenically driven climate change is affecting heat waves and drought is one of the most important environmental issues facing societies around the globe. Zhang *et al.* present a 260-year-long record of temperature and soil moisture over inner East Asia that reveals an abrupt shift to hotter and drier conditions (see the Perspective by Zhang and Fang). Extreme episodes of hotter and drier climate over the past 20 years, which are unprecedented in the earlier records, are caused by a positive feedback loop between soil moisture deficits and surface warming and potentially represent the start of an irreversible trend.

Science, this issue p. 1095; see also p. 1037